MATERIALS

Erbium(III) acetate hydrate (99.9%), thulium(III) acetate hydrate (99.9%), Neodymium(III) acetate hydrate (99.9%), ytterbium(III) acetate tetrahydrate (99.9%), yttrium(III) acetate hydrate (99.9%), oleic acid (technical grade, 90%), 1-octadecene (technical grade, 90%), ammonium fluoride (99.99+%), 2,3,3-trimethyl-3H-indole, 1-iodopropane and 2-hydroxy-5-nitrobenzaldehyde, these chemicals were purchased from Sigma-Aldrich. All chemicals were used as received, without any further purification. Solvents for NMR analysis (Cambridge Isotope Laboratories) were used as received.

METHODS

UV-vis absorption spectra were recorded on a Varian Cary 50 spectrophotometer. Fluorescence spectra were record on a Varian Cary Eclipse fluorescence spectrophotometer with external NIR lasers with a wavelength at 808 nm or 980 nm as excitation light source (CNI high power fiber coupled diode laser system, FC-W-980 and FC-W-808). The total output powers for the lasers are tunable from 1 mW to 10 W. The power density was detected by 1916-R handheld optical power meter with 818P thermophile detector (purchased from Newport corporation, USA) Unless otherwise stated, all spectra were obtained from hexane dispersion of nanoparticles (1 wt%). Fluorescence emission decays of UCNPs were collected on a Edinburgh FLS920 fluorescence spectrometer with a external continuous 980 nm NIR LED laser diode (1.5 W), which was coupled with a chopper to modulated the excitation into pulse mode . ^{1}H NMR and ^{13}C NMR was acquired on Varian 300MHz NMR spectrometer. Low resolution transmission electron microscopy (TEM) was performed on a Topcon 002B electron microscope at 200 kV. High resolution TEM, Scanning Transmission Electron Microscopy (STEM) and energy-dispersive X-ray spectroscopy (EDX) spectrum were performed on a JEOL-JEM 2100F electron microscope. Sample preparation was carried out by placing a drop of the freshly prepared colloidal solution on a carbon-coated copper grid and allowing the solution to evaporate. Luminescence digital photographs were taken with a Nikon D3000 camera.

SYNTHESIS

(1) Synthesis of UCNPs

The multi-shells structured nanoparticles were synthesized via a modified recently reported procedure.[S1]

Synthesis of core *β*-$NaYF_4$: 1 mol% Nd^{3+}, 30 mol% Yb^{3+}, 0.5 mol% Tm^{3+} nanoparticles (*β*-$NaYF_4$:Nd^{3+}/Yb^{3+}/Tm^{3+}). $Y(CH_3CO_2)_3 \cdot xH_2O$ (1.37 mmol), $Nd(CH_3CO_2)_3 \cdot xH_2O$ (0.02 mmol), $Yb(CH_3CO_2)_3 \cdot xH_2O$ (0.6 mmol), and $Tm(CH_3CO_2)_3 \cdot xH_2O$ (0.01 mmol) were added to a 100-mL flask containing 12 mL of oleic acid and 15 mL of 1-octadecene. The mixture was heated at 130 °C for 30 min under vacuum to form the lanthanide-oleate complexes and remove water. Then the solution was cooled down to 50 °C naturally under argon. Thereafter, 12 mL of methanol solution containing NH_4F (8 mmol) and NaOH (5 mmol) was added and the resultant solution was stirred for 30 min. After the methanol was evaporated, the solution was heated to 300 °C under argon for 90 min and then cooled down to room temperature. The resulting nanoparticles were precipitated by addition of ethanol, collected by centrifugation at 3000 rpm for 5 min, washed with ethanol several times, and re-dispersed in 10 mL of hexane.

Synthesis of core-shell *β*-$NaYF_4$: 1 mol% Nd^{3+}, 30 mol% Yb^{3+}, 0.5 mol% Tm^{3+}@*β*-$NaYF_4$: 20 mol% Nd^{3+} nanoparticles (*β*-$NaYF_4$:Nd^{3+}/Yb^{3+}/Tm^{3+}@*β*-$NaYF_4$:Nd^{3+}). $Y(CH_3CO_2)_3 \cdot xH_2O$ (1.44 mmol) and $Nd(CH_3CO_2)_3 \cdot xH_2O$ (0.36 mmol) were added to a 100-mL flask containing 12 mL of oleic acid and 15 mL of 1-octadecene. The mixture was heated at 130 °C for 30 min under vacuum to form the lanthanide-oleate complexes and remove water. Then the solution was lowered to 80 °C under argon and the dispersion of β-$NaYF_4$:Nd^{3+}/Yb^{3+}/Tm^{3+} core nanoparticles in hexanes was added. The resulting solution was heated 90 °C to remove the hexane. Then the solution was cooled down to 50 °C and 10 mL of methanol solution containing NH_4F (7.2 mmol) and NaOH (4.5 mmol) was added and the resultant solution was stirred for 30 min. After the methanol was evaporated, the solution was heated to 300 °C under argon for 90 min and then cooled down to room temperature. The resulting nanoparticles were precipitated by addition of ethanol, collected by centrifugation at 3000 rpm for 5 min, washed with ethanol several times, and re-dispersed in 10 mL of hexane.

Synthesis of core-shell(II) *β*-$NaYF_4$: 1 mol% Nd^{3+}, 30 mol% Yb^{3+}, 0.5 mol% Tm^{3+}@*β*-$NaYF_4$: 20 mol% Nd^{3+}@*β*-$NaYF_4$ nanoparticles (*β*-$NaYF_4$:Nd^{3+}/Yb^{3+}/Tm^{3+}@*β*-$NaYF_4$:Nd^{3+}@*β*-$NaYF_4$). The same procedure outlined above for the synthesis of *β*-$NaYF_4$:Nd^{3+}/Yb^{3+}/Tm^{3+}@β-$NaYF_4$:Nd^{3+} core-shell nanoparticles was employed except that the core-shell nanoparticle was used as core and $Y(CH_3CO_2)_3 \cdot xH_2O$ was used as precursor for epitaxial shell growth.

Synthesis of core-shell(III) *β*-$NaYF_4$: 1 mol% Nd^{3+}, 30 mol% Yb^{3+}, 0.5 mol% Tm^{3+}@*β*-$NaYF_4$: 20 mol% Nd^{3+}@*β*-$NaYF_4$@*β*-$NaYF_4$: 18 mol% Yb^{3+}, 2 mol% Er^{3+} nanoparticles (*β*-$NaYF_4$:Nd^{3+}/Yb^{3+}/Tm^{3+}@*β*-$NaYF_4$:Nd^{3+}@*β*-$NaYF_4$@$NaYF_4$: Yb^{3+}/Er^{3+}, Tm@Er). The same procedure outlined above for the synthesis of *β*-$NaYF_4$:Nd^{3+}/Yb^{3+}/Tm^{3+}@*β*-$NaYF_4$:Nd^{3+}@*β*-$NaYF_4$ core-shell(II) nanoparticles was employed except that the core-shell(II) nanoparticle was used as core and $Y(CH_3CO_2)_3 \cdot xH_2O$, $Yb(CH_3CO_2)_3 \cdot xH_2O$ and $Er(CH_3CO_2)_3 \cdot xH_2O$ were used as precursors for epitaxial shell growth.

Synthesis of core *β*-$NaYF_4$: 0.5 mol% Nd^{3+}, 20 mol% Yb^{3+}, 2 mol% Tm^{3+} nanoparticles (*β*-$NaYF_4$:Nd^{3+}/Yb^{3+}/Er^{3+}). The same procedure outlined above for the synthesis of *β*-$NaYF_4$:Nd^{3+}/Yb^{3+}/Er^{3+} core nanoparticles was employed except that the $Y(CH_3CO_2)_3 \cdot xH_2O$, $Nd(CH_3CO_2)_3 \cdot xH_2O$, $Yb(CH_3CO_2)_3 \cdot xH_2O$ and $Er(CH_3CO_2)_3 \cdot xH_2O$ were used as precursors.

Synthesis of core-shell *β*-$NaYF_4$: 0.5 mol% Nd^{3+}, 20 mol% Yb^{3+}, 2 mol% Tm^{3+}@*β*-$NaYF_4$: 20 mol% Nd^{3+} nanoparticles (*β*-$NaYF_4$:Nd^{3+}/Yb^{3+}/Er^{3+}@*β*-$NaYF_4$:Nd^{3+}). The same procedure outlined above for the synthesis of *β*-$NaYF_4$:Nd^{3+}/Yb^{3+}/Tm^{3+}@β-$NaYF_4$:Nd^{3+} core-shell nanoparticles was employed except that the *β*-$NaYF_4$:Nd^{3+}/Yb^{3+}/Er^{3+} core nanoparticle was used as core.

Synthesis of core-shell(II) *β*-$NaYF_4$: 0.5 mol% Nd^{3+}, 20 mol% Yb^{3+}, 2 mol% Tm^{3+}@*β*-$NaYF_4$: 20 mol% Nd^{3+}@*β*-$NaYF_4$ nanoparticles (*β*-$NaYF_4$:Nd^{3+}/Yb^{3+}/Er^{3+}@*β*-$NaYF_4$:Nd^{3+}@*β*-$NaYF_4$). The same procedure outlined above for the synthesis of *β*-$NaYF_4$:Nd^{3+}/Yb^{3+}/Tm^{3+}@β-$NaYF_4$:Nd^{3+}@*β*-$NaYF_4$ core-shell(II) nanoparticles was employed except that the *β*-$NaYF_4$:Nd^{3+}/Yb^{3+}/Er^{3+}@β-$NaYF_4$:Nd^{3+} core-shell nanoparticle was used as core.

Synthesis of core-shell(III) *β*-$NaYF_4$: 0.5 mol% Nd^{3+}, 20 mol% Yb^{3+}, 2 mol% Tm^{3+}@*β*-$NaYF_4$: 20 mol% Nd^{3+}@*β*-$NaYF_4$@*β*-$NaYF_4$: 30 mol% Yb^{3+}, 0.5 mol% Tm^{3+} nanoparticles (*β*-$NaYF_4$:Nd^{3+}/Yb^{3+}/Er^{3+}@*β*-$NaYF_4$:Nd^{3+}@*β*-$NaYF_4$@$NaYF_4$: Yb^{3+}/Tm^{3+}, Er@Tm). The same procedure outlined above for the synthesis of *β*-$NaYF_4$:Nd^{3+}/Yb^{3+}/Tm^{3+}@β-$NaYF_4$:Nd^{3+}@*β*-$NaYF_4$@*β*-$NaYF_4$@$NaYF_4$: Yb^{3+}/Er^{3+} core-shell(III) nanoparticles was employed except that the *β*-$NaYF_4$:Nd^{3+}/Yb^{3+}/Er^{3+}@β-$NaYF_4$:Nd^{3+}@*β*-$NaYF_4$ core-shell(II) nanoparticle was used as core and $Yb(CH_3CO_2)_3 \cdot xH_2O$ and $Tm(CH_3CO_2)_3 \cdot xH_2O$ were used as precursors.

Synthesis of core-shell(IV) Tm@Er@ *β*-$NaYF_4$ and Er@Tm@ *β*-$NaYF_4$ nanoparticles. The same procedure outlined above for the synthesis of *β*-$NaYF_4$:Nd^{3+}/Yb^{3+}/Tm^{3+}@β-$NaYF_4$ core-shell(II) nanoparticles was employed except that the Tm@Er or Er@Tm nanoparticle was used as core.

(2) Synthesis of UCNPs@mesoporous silica core-shell nanoparticle, UCNPs@MSNs

In a typical procedure, 40 mg UCNPs in chloroform (1 mL) were poured into aqueous CTAB solution (10 mL, 360 mg), and the resulting solution was sonicated by using a probe-type sonicator at 400 W for 30 min to result in a transparent UCNPs@CTAB solution. The nanoparticles were collected by centrifugation and were re-dispersed in 1 mL water. The cenctrifugation/re-dispersion procedure was repeated 3 times to remove the excess amount of CTAB. Thereafter, the UCNPS@CTAB solution (1 mL) was added to a CTAB solution (9 mL, 8.2 mg/mL) and NaOH solution (0.1 mL, 0.1 M). The mixture was stirred at for 30 min and 50 μL of TEOS was added. The mixture was further stirred at 55 °C for 4 h and the as-syntesized UCNPs@MSNs were collected by centrifugation and washed with methanol 3 times. The CTAB surfactant template was then extracted with a 1 wt% HCl solution in methanol.

(3) Synthesis of 1-(2-propyl)-3,3-dimethylindolino-6'-nitrobenzopyrylospiran, SP

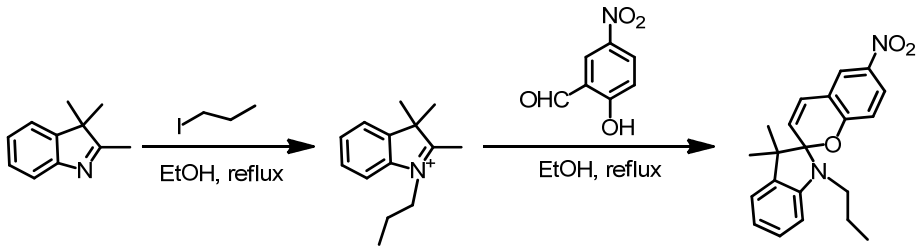

Synthesis of 1-propyl-2,3,3-trimethyl-3H-indolium iodide.[S2] To a solution of 2,3,3-trimethyl-3H-indole (1.0 g, 6.25 mmol) in 5 mL acetone, 1-iodopropane (5.3 mL, 31 mmol) was added, and refluxed with continuous stirring for 15 h. The mixture was dried under high vacuum and washed with diethyl ether. The resulting solid was re-crystallized in acetone to obtain the product as a pink solid.

1H-NMR (300 MHz, DMSO-d_6): 1.04 (t, 3H, J = 7.2 Hz), 1.34 (m, 2H), 1.64 (s, 6H), 2.67 (s, 3H), 4.17 (t, 2H, J = 7.8 Hz), 7.63 (d, 2H, J = 7.4 Hz), 7.82 (m, 2H). ESI m/z calc: 202.4; found: 202.1.

Synthesis of 1-(2-propyl)-3,3-dimethylindolino-6'-nitrobenzopyrylospiran, SP. To a solution of 1-propyl-2,3,3-trimethyl-3H-indole (1.0 g) in 15 mL dry ethanol, 2-hydroxy-5-nitrobenzaldehyde (0.85g) was added, and refluxed with continuous stirring for overnight. The mixture was dried under high vacuum and was purified by flash chromatography on a silica gel column using DCM as eluent.

1H-NMR (400 MHz, DMSO-d_6): 0.91 (t, 3H, J = 9.6 Hz), 1.19 (s, 3H), 1.29 (s, 3H), 1.64 (m, 2H), 3.12 (t, 2H), 7.08 (d, 1H, J = 9.6 Hz), 7.18 (t, 1H, J = 10 Hz), 8.02 (n, 2H). 13C-NMR (400 MHz, DMSO-d_6): 11.77, 19.87, 22.19, 26.04, 45.46, 52.68, 106.68, 106.80, 115.54, 118.52, 119.27, 121.67, 122.13, 122.71, 125.88, 127.75, 128.04, 135.93, 140.89, 147.25, 159.76.

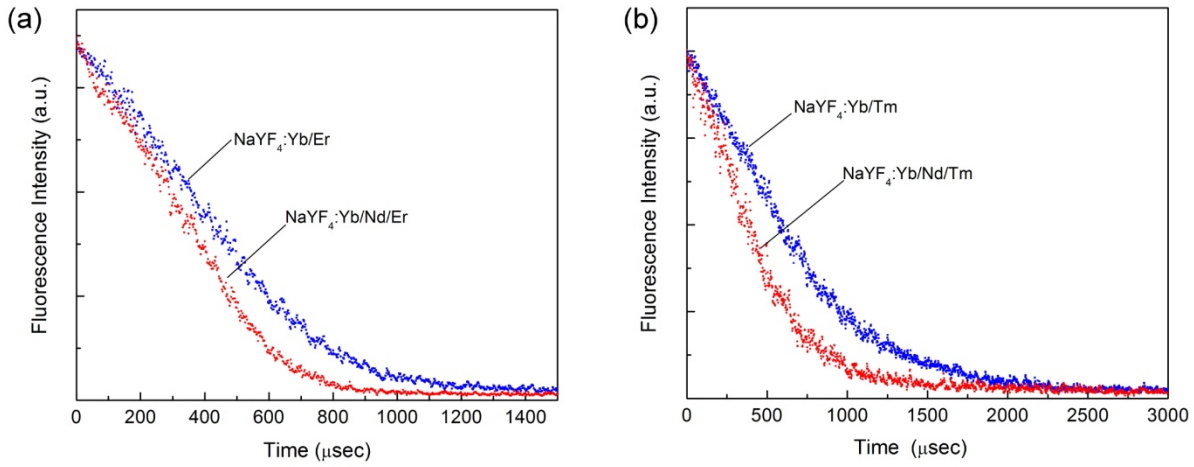

FIGURE S1. Fluorescence emission decay of $NaYF_4$:Yb/Er (a) and $NaYF_4$:Yb/Tm (b) UCNPs co-doped with/without Nd^{3+} (1 mol%). The emission decay was collected at 540 nm and 473 nm for Er and Tm UCNPs, respectively, under 980 nm excitation. It clearly shows that doping of Nd^{3+} shortens the fluorescence lifetime for both Er^{3+} and Tm^{3+} UNCPs, due to enhanced cross-relaxation between Nd^{3+} and locally positioned activators, which manifests as fluorescence quenching of the UCNPs. This characteristic endows the Nd^{3+} doped UCNP with an excitation at 808 nm responsive to high power density; however, the UCNPs will not be excited by low power density 980 nm NIR light. This has also been demonstrated by Han's group, where the Nd^{3+} concentration was proportional to fluorescence quenching of the UCL under 980 nm excitation (see ref. [8h], Figure S20).

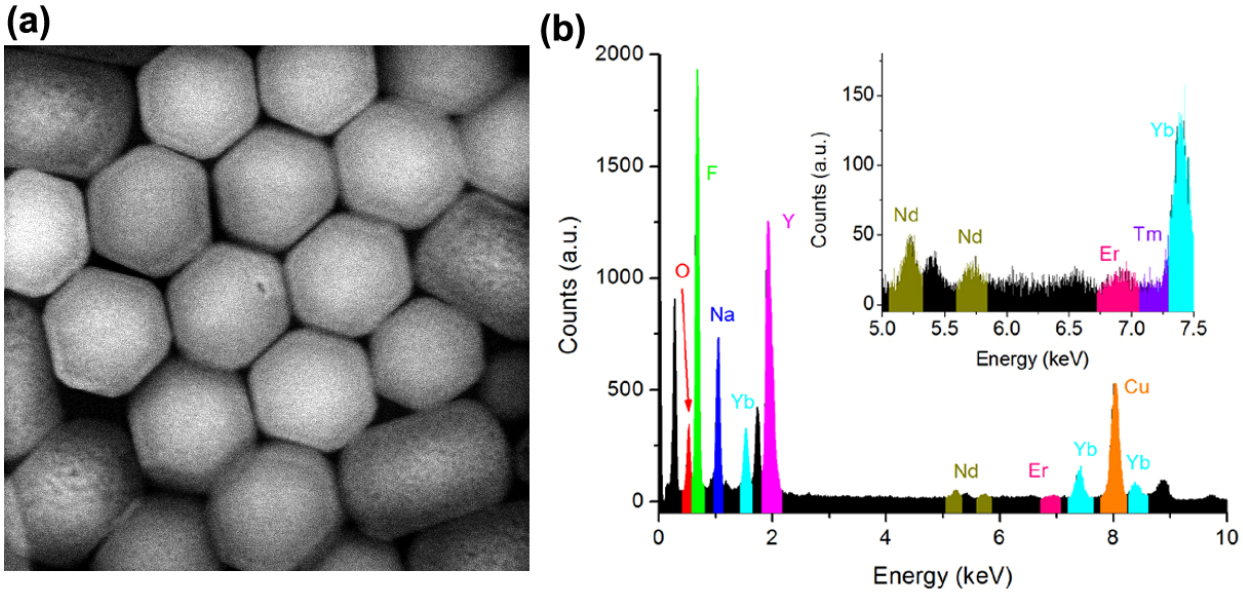

FIGURE S2. (a) High-angle annular dark field STEM image and (b) Energy-dispersive X-ray spectroscopy (EDX) spectrum of the **Tm@Er** nanoparticles.

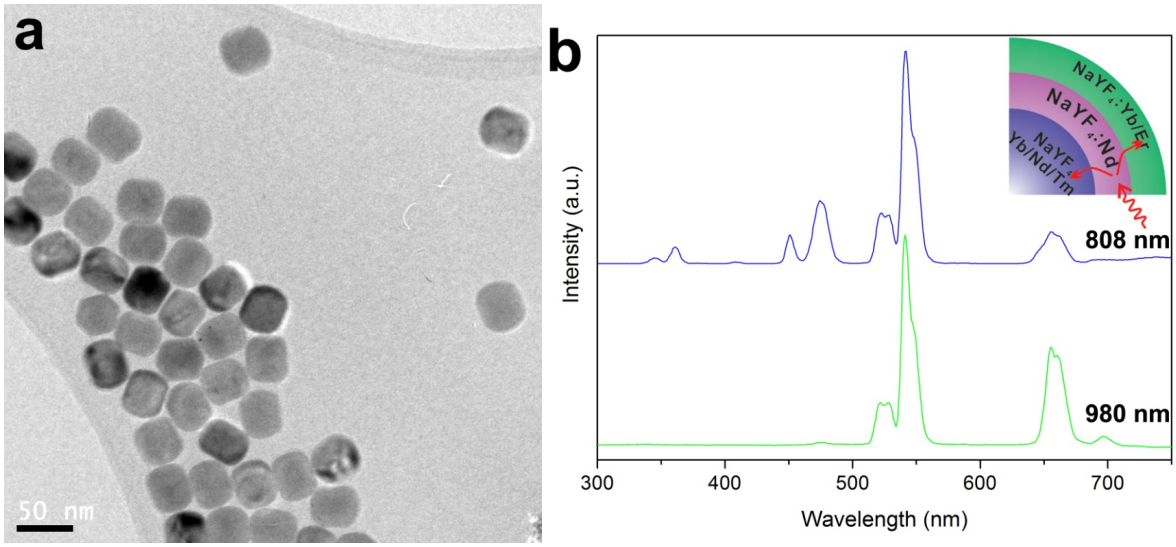

FIGURE S3. (a) TEM image of β-$NaYF_4$:Nd^{3+}/Yb^{3+}/Tm^{3+}@$NaYF_4$:Nd^{3+}@$NaYF_4$:Yb^{3+}/Er^{3+} nanoparticles, which lacks a photon inert shell as compared to the **Tm@Er** nanoparticles. (b) Upconversion luminescence of the desired nanoparticles under NIR lasers excitation with different wavelengths (1 wt% in hexane solution). For 808 nm excitation, the nanoparticles show strong energy migration from the Nd^{3+} sensitized shell to both the inner luminescent core and outer luminescent shell, and thus display the characteristic emission peaks of both Tm^{3+} and Er^{3+}. The relatively lower emission of Tm^{3+}, as compared to Er^{3+}, is mainly due to quenching effect of Nd^{3+} doped in the luminescent core. As for 980 nm excitation, using a low power density allows for the selective excitation of the outer shell and thus leads to only Er^{3+} emission.

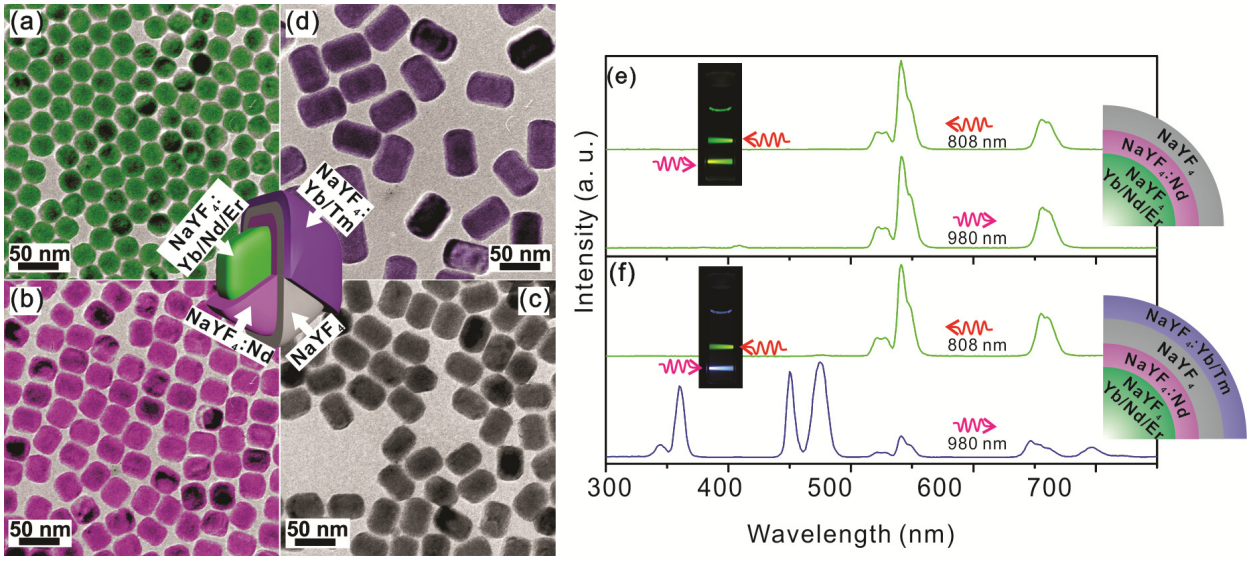

FIGURE S4. Similar to the synthesis of **Tm@Er** UNCPs, the synthesis of **Er@Tm** UNCPs begins with the synthesis of the initial core containing NaYF4:Yb/Nd/Er, followed by epitaxial growth of the Nd^{3+} abundant shell, the photon inert shell, and finally the luminescent outer shell(Yb/Tm). TEM characterizations (**a-d**) reveal similar changes in size and morphology as compared to the growth of Tm@Er UNCPs. Upconversion luminescence spectra show that the Er-doped core displays the characteristic emission peaks of Er under both 980 nm and 808 nm excitation (Figure S3e), evident as two green bands in hexanes solution (1 wt%) from 980 nm and 808 nm laser excitation with a power density of 60 $W \cdot cm^{-2}$ (Figure. S3e, inset). For the **Er@Tm** UNCPs, the 808 nm excitation induced green emission from Er^{3+} indicates that only the core can be excited by 808 nm excitation. However, the 980 nm laser stimulated not only UV to blue emissions from the Tm^{3+} in the shell, but also green emission from Er^{3+} in the core (Figure S3f). The relatively lower green emission from Er^{3+} is due to the enhanced cross-relaxation between Nd^{3+} and Er^{3+}, which results in a quenching of the UCL in the **LC**. The structures of the corresponding nanoparticles are illustrated on the right panel.

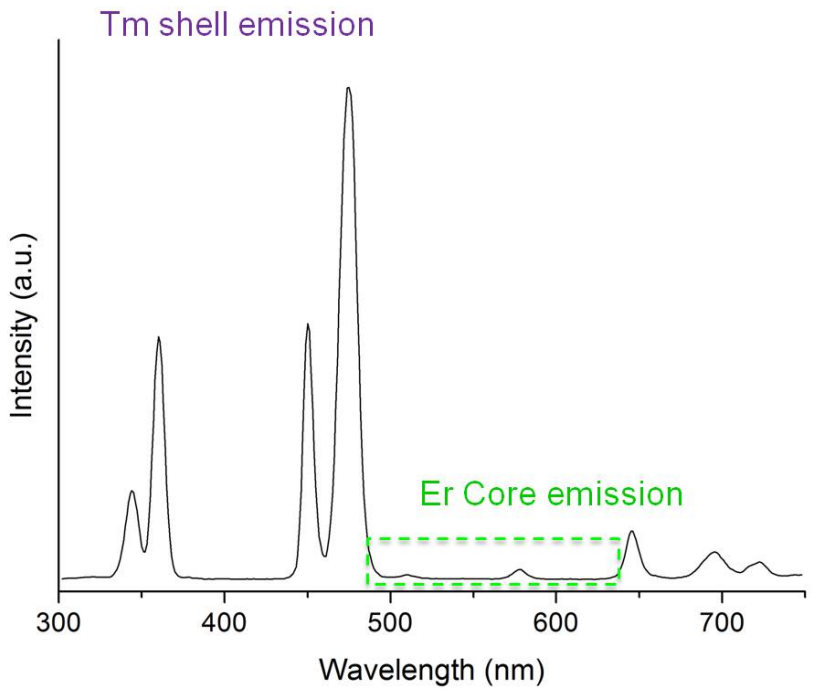

FIGURE S5. UCL emission of **Er@Tm** nanoparticle excited by a 980 nm NIR laser with a relatively low power density (18 $W \cdot cm^{-2}$). Comparing to the emission spectrum shown in Figure S3f, the unwanted Er^{3+} emission from the core was reduced with a lower power density of excitation. However, the UV emission (365 nm) from the luminescent shell also decreased in intensity, which can be seen by comparing its relative intensity to the intensity of the blue emission from Tm at 475 nm. It should be noted that the UV emission decreased in intensity more quickly than the blue emissions. This is due to the non-linear nature of the upconversion of 980 nm light to 365 nm and 475 nm which requires the sequential absorption of 4 to 5 or 3 photons, respectively. As such, the upconversion to UV light exhibits a stronger dependence on the excitation power density than that of visible light.

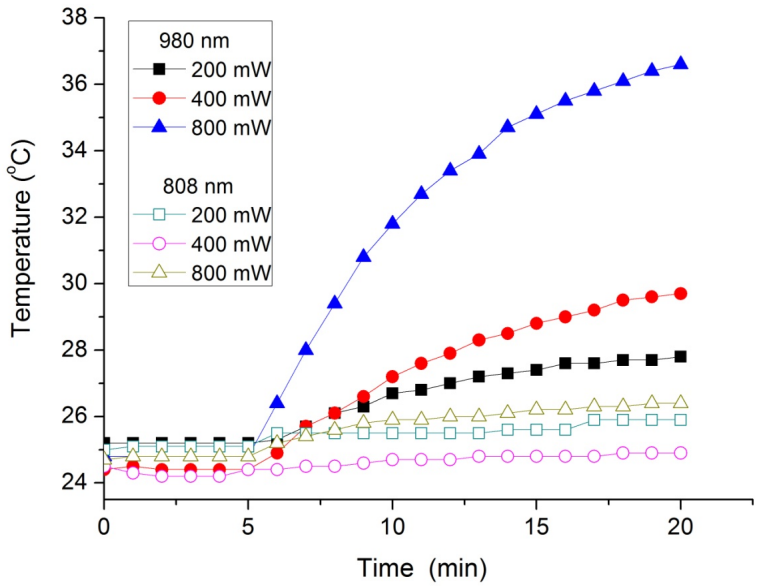

FIGURE S6. Heating effect of the laser using different wavelengths and power. The experiments were carried out by irradiating the laser on a standard fluorescence quartz cuvette with 1.5 mL water and a laser path of 1 cm. Laser beam has a diameter of ca. 1 mm. The solution was kept in room temperature for 5 min for balance then the laser was turned on. The output power of the laser was adjustable and was determined by a laser power meter. It shows that the 980 nm laser has a higher heating effect than 808 nm laser, which is especially significant when using high power irradiation.

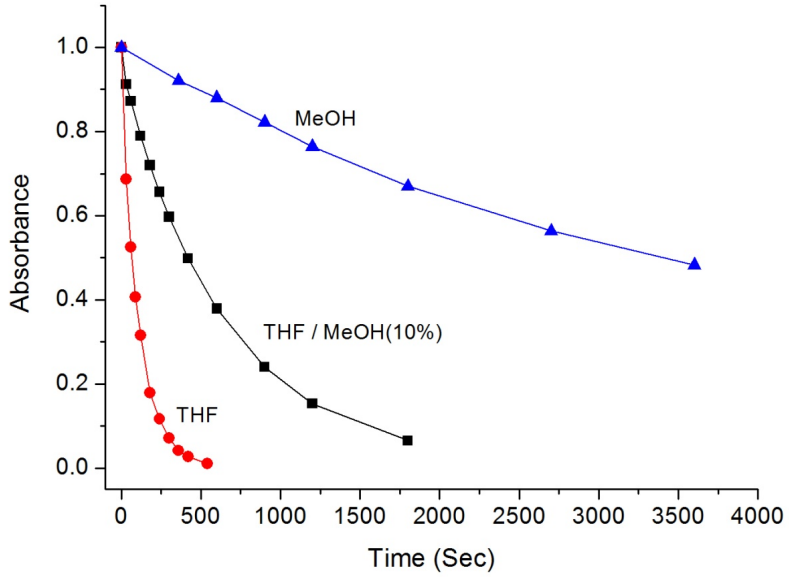

FIGURE S7. Kinetic study for the isomerization of ME to SP in dark condition in different solvents. Data were recorded by monitoring the absorbance of the characteristic absorption peak of **ME** at 560 nm. It shows that **ME** in THF has faster isomerization kinetics than in methanol (MeOH). Due to the hydrophobic nature of the as synthesized UCNP, it is highly soluble in THF but cannot be dispersed in MeOH. Thus in this study, a mixture of THF/MeOH (10%) was chose for the photoswitching study, in which **ME** to **SP** reaction displays relatively slow reaction kinetics in the dark and the UCNPs have good solubility.

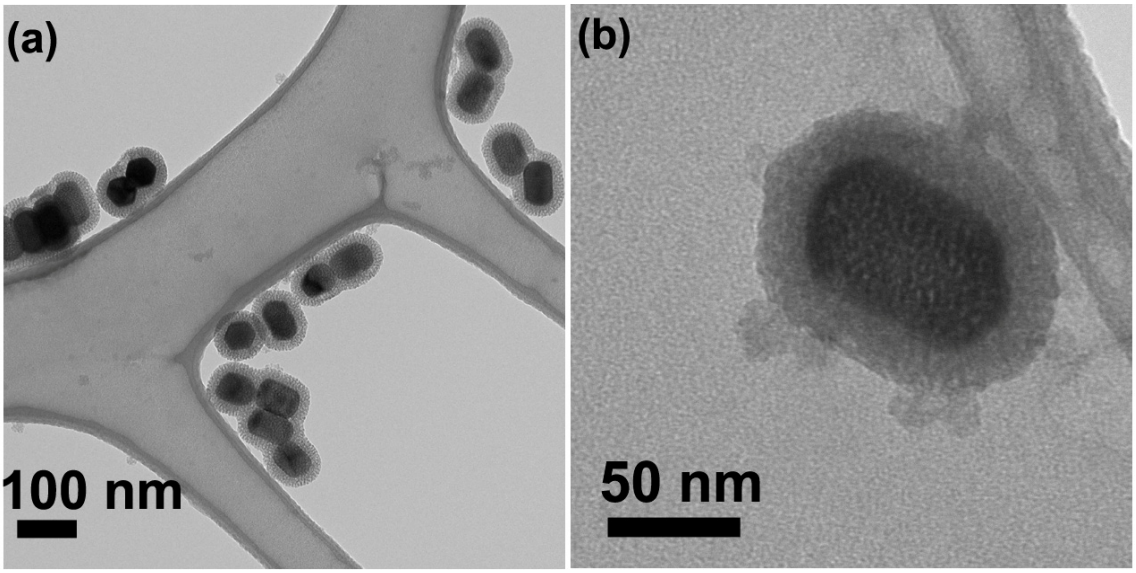

FIGURE S8. TEM images of UCNP@MSNs nanoparticles.

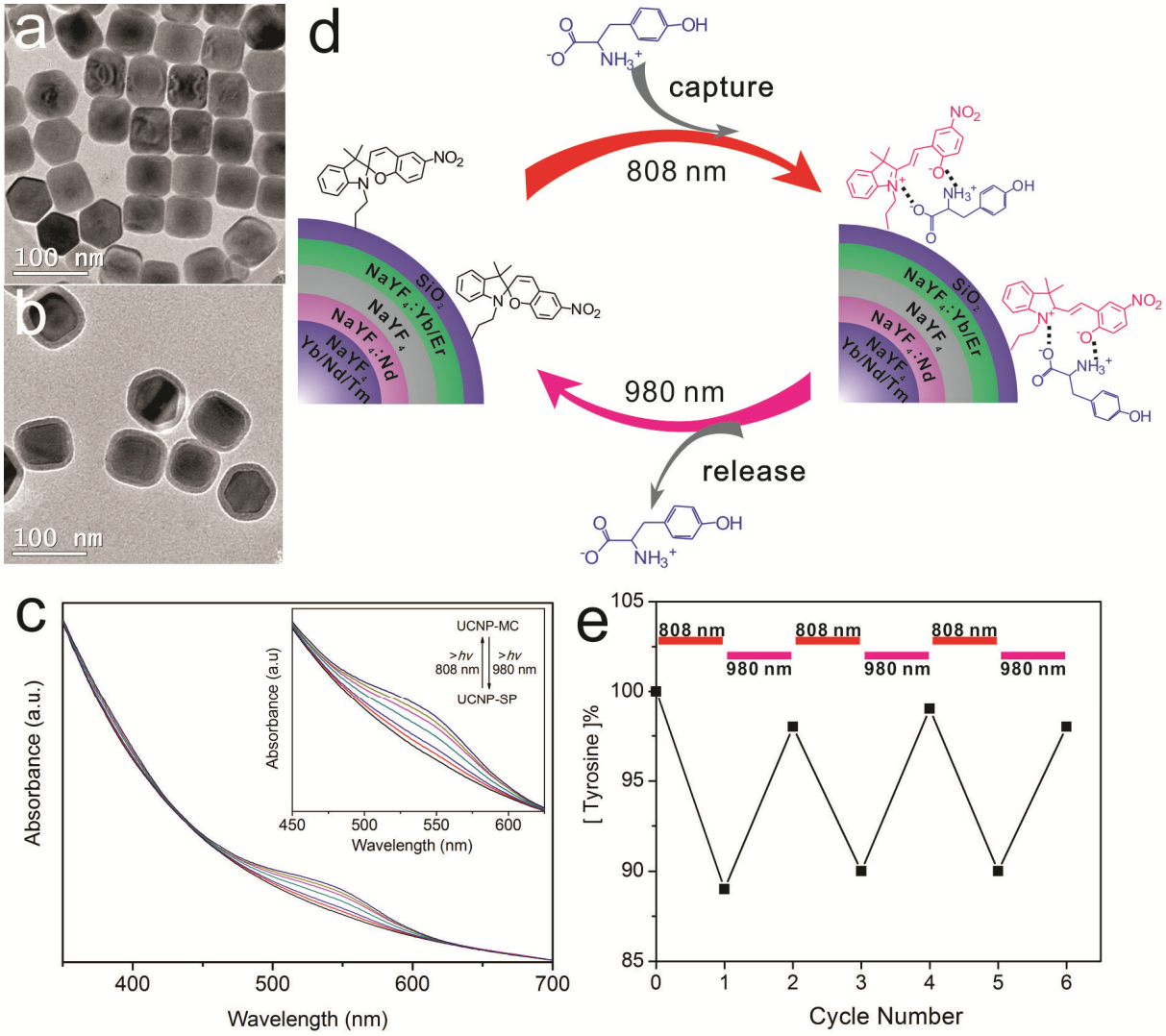

FIGURE S9: (a-b) TEM images of **Tm@Er** and **Tm@Er@SiO$_2$** nanoparticles. (c) Absorption spectrum characterization of the photoswitching of UCNP-SP in methanol solution using 808 nm and 980 nm NIR light. (d) Schematic illustration of dual NIR light regulated capture and release of tyrosine using UCNP-SP in solution and (e) the change in tyrosine content in solution along NIR light irradiation (20 uM tyrosine and 10 mg UCNP-SP in 2 mL methanol solution. Irradiation condition for 808 nm and 980 nm laser is 60 W·cm^{-2}, 4 min and 25 W·cm^{-2}, 3 min, respectively.)

To further demonstrate the advantage and utility of our core-shell multicolor nanoparticles, herein we provide preliminary results for the construction of a single UCNP-based dual NIR light responsive drug delivery system. We first prepared spiropyran functionalized silica shell coated **Tm@Er** UCNP (UCNP-SP, see Figure S9, a-b). Similar to the previous results (Figure 4), the reversible photoswitching of spiropyran between its **SP** and **MC** form can be effectively triggered using two NIR excitations (808 nm and 980 nm) in solution (Figure S9c). It should be noted that the efficiency of photoswitching has been improved due to the attachment of **SP** to the UNCP surface (lower power density and shorter irradiation are used). It has been previously demonstrated that amino acids such as L-tyrosine and L-

DOPA bind to the zwitterionic **MC** and can be subsequently released upon irradiation with visible light, where the **MC** isomerizes to the nonpolar **SP** form.[S3] We then demonstrated the reversible capture and release of L-tyrosine in solution using the UCNP-SP and applying low power 808 nm and 980 nm NIR light, respectively (Figure S9, d-e). However, in contrast, such a complete capture and release cycle cannot be observed by using a mixture of two single color UCNPs (Er-SP and Tm-SP) under the same experimental conditions (UCNP concentration, irradiation time and power density), because only half of the UCNPs (one type, either Er-SP or Tm-SP) in the mixture can be excited at one time and SP will proceed *via* a one-way photoisomerization on the nanoparticle surface each time (data not shown). The detailed project is currently being developed in our lab, but these preliminary results clearly demonstrate the higher spatial control achievable with our core-shell UCNPs over admixtures of monochromatic UCNPs, especially under low power density 980 nm excitation.

KEY REFERENCES FOR SUPPROTING INFORMATION:

[S1] X. Xie, N. Gao, R. Deng, Q. Sun, Q.-H. Xu, X. Liu, *J. Am. Chem. Soc.* **2013**, 135, 12608.

[S2] A. Samanta, K. K. Maiti, K. S. Soh, X. Loiao, M. Vendrell, U. S. Sinish, S. W. Yun, R. Bhuvaneswari, H. Kim, S. Rautela, J. Chung, M. Olivo, Y. T. Chang, *Angew. Chem. Int. Ed.* **2011**, *50*, 6089.

[S3] B. I. Ipe, S. Mahima, K. G. Thomas, *J. Am. Chem. Soc.* **2003**, *125*, 7174.